Spectroscopic quadrupole moments in ^{124}Xe

E. Clément,[1] A. Lemasson,[1] M. Rejmund,[1] B. Jacquot,[1] D. Ralet,[1] C. Michelagnoli,[1,2] D. Barrientos,[3] P. Bednarczyk,[4] G. Benzoni,[5] A. J. Boston,[6] A. Bracco,[5,7] B. Cederwall,[8] M. Ciemala,[4] J. Collado,[9,10] F. Crespi,[7,5] C. Domingo-Pardo,[11] J. Dudouet,[12] H. J. Eberth,[13] G. de France,[1] A. Gadea,[11] V. Gonzalez,[9] A. Gottardo,[10] L. Harkness,[6] H. Hess,[13] A. Jungclaus,[14] A. Kaşkaş,[15] W. Korten,[16] S. M. Lenzi,[17,18] S. Leoni,[5,7] J. Ljungvall,[19] R. Menegazzo,[17] D. Mengoni,[17,18] B. Million,[5] D. R. Napoli,[10] J. Nyberg,[20] Zs. Podolyak,[21] A. Pullia,[5,7] B. Quintana Arnés,[22] F. Recchia,[17,18] N. Redon,[12] P. Reiter,[13] M. D.Salsac,[16] E. Sanchis,[9] M. Şenyiğit,[15] M. Siciliano,[10,16,23] D. Sohler,[24] O. Stezowski,[12] C. Theisen,[16] and J. J. Valiente Dobón[10]

[1]*GANIL, CEA/DRF-CNRS/IN2P3, Bd. Henri Becquerel, BP 55027, F-14076 Caen, France*
[2]*Institut Laue-Langevin, B.P. 156, F-38042 Grenoble Cédex 9, France*
[3]*CERN, CH-1211 Geneva 23, Switzerland*
[4]*The Henryk Niewodniczanski Institute of Nuclear Physics, Polish Academy of Sciences, ul. Radzikowskiego 152, 31-342 Krakow, Poland*
[5]*Istituto Nazionale di Fisica Nucleare, Milano, I-20133 Milano, Italy*
[6]*Oliver Lodge Laboratory, The University of Liverpool, Oxford Street, Liverpool L69 7ZE, United Kingdom*
[7]*Dipartimento di Fisica, Universitá di Milano, I-20133 Milano, Italy*
[8]*Department of Physics, KTH Royal Institute of Technology, SE-10691 Stockholm, Sweden*
[9]*Department of Electronic Engineering, University of Valencia, E-46100 Burjassot Valencia, Spain*
[10]*INFN, Laboratori Nazionali di Legnaro, I-35020 Legnaro, Padova, Italy*
[11]*Istituto de Física Corpuscular, CSIC-Universidad de Valencia, E-46071 Valencia, Spain*
[12]*Université de Lyon, Université Lyon-1, CNRS/IN2P3, UMR5822, IP2I, 4 Rue Enrico Fermi, F-69622 Villeurbanne Cedex, France*
[13]*Institut für Kernphysik, Universität zu Köln, Zülpicher Str. 77, D-50937 Köln, Germany,*
[14]*Istituto de Estructura de la Materia, CSIC, E-28006 Madrid, Spain*
[15]*Department of Physics, Faculty of Science, Ankara University, 06100 Besevler - Ankara, Turkey*
[16]*Irfu, CEA, Université Paris-Saclay, F-91191 Gif-sur-Yvette, France*
[17]*Istituto Nazionale di Fisica Nucleare, Sezione di Padova, I-35131 Padova, Italy*
[18]*Dipartimento di Fisica e Astronomia dell'Universitá di Padova, I-35131 Padova, Italy*
[19]*Université Paris-Saclay, CNRS/IN2P3, IJCLab, 91405 Orsay, France*
[20]*Department of Physics and Astronomy, Uppsala University, SE-75120 Uppsala, Sweden*
[21]*Department of Physics, University of Surrey, Guildford GU2 7XH, United Kingdom*
[22]*Laboratorio de Radiaciones Ionizantes, Departamento de Física Fundamental, Universidad de Salamanca, E-37008 Salamanca, Spain*
[23]*Physics Division, Argonne National Laboratory, Argonne, Illinois 60439, USA*
[24]*Institute for Nuclear Research, Atomki, 4001 Debrecen, P.O. Box 51, Hungary*

(Received 21 October 2022; accepted 23 January 2023; published 30 January 2023)

Background: The Xe isotopic chain with four valence protons above the $Z = 50$ shell closure is an ideal laboratory for the study of the evolution of nuclear deformation. At the $N = 82$ shell closure, ^{136}Xe presents all characteristics of a doubly closed shell nucleus with a spherical shape. In the very neutron-deficient isotopes close to $N = 50$, the α-decay chain of Xe was investigated to probe the radioactive decay properties near the drip-line and the magicity of ^{100}Sn. Additionally, the Xe isotopes present higher order symmetries in the nuclear deformation such as the octupole degree of freedom near $N = 60$ and $N = 90$ or O(6) symmetry in stable isotopes.

Purpose: The relevance of the O(6) symmetry has been investigated by measuring the spectroscopic quadrupole moment of the first excited states in ^{124}Xe. In the O(6) symmetry limit, the spectroscopic quadrupole moment of collective states is expected to be null.

Method: A stable ^{124}Xe beam with energies of 4.03A MeV and 4.11A MeV was used to bombard a $^{\text{nat}}$W target at the GANIL facility. Excited states were populated via the safe Coulomb excitation reaction. The collision of the heavy ions with a large Z at low energy make this reaction sensitive to the diagonal $E2$ matrix element of the excited states. The recoils were detected in the VAMOS++ magnetic spectrometer and the γ rays in the AGATA tracking array. The least squares fitting code GOSIA was used for the analysis to extract both $E2$ and $M1$ transitional and $E2$ diagonal matrix elements.

Results: The rotational ground state band was populated up to the 8_1^+ state as well as the 2_2^+ and 4_2^+ states. Using high precision spectroscopic data to constrain the GOSIA fit, the spectroscopic quadrupole moments of the 2_1^+, 4_1^+, and 6_1^+ states were determined for the first time.

 ©2023 American Physical Society

Conclusions: The spectroscopic quadrupole moments were found to be negative, large, and constant in the ground state band underlining the prolate axially deformed ground state band of ^{124}Xe. The present experimental data confirm that the O(6) symmetry is substantially broken in ^{124}Xe.

DOI: 10.1103/PhysRevC.107.014324

I. INTRODUCTION

With four protons added to the $Z = 50$ shell closure, the Xe isotopes are an ideal laboratory to investigate the collective properties of the nuclear matter. On the neutron-rich side, ^{136}Xe highlights the $N = 82$ shell closure with a maximum excitation energy of the 2_1^+ state and a minimum in the corresponding reduced transition probability $B(E2, 2_1^+ \rightarrow 0_1^+)$ [1]. When removing neutrons from $N = 82$, the Xe isotopes follow a smooth increase of collectivity reaching a maximum at midshell around $N = 66$ [2]. In these isotopes, low excitation energies of the 2_1^+ states, rotational ground state bands and large $B(E2)$ values were reported. Approaching the $N = 50$ shell closure, an unexpected onset of collectivity was observed in ^{110}Xe [3]. Beyond the quadrupole symmetry, harmonic octupole correlations have been identified associated with the collective 3^- states at low excitation energy at the midshell [4], whereas in the neutron deficient ^{114}Xe isotope an unexpectedly large $B(E3, 3^- \rightarrow 0_1^+)$ was measured [5].

The collective properties of the stable Xe isotopes have been scrutinized in the light of dynamical symmetries to describe the transition from spherical shape at the closed shells to large deformation in the midshell region. The transition region should involve γ-soft and γ-rigid deformation [6,7]. Fingerprints of such deformations were observed in the even-A mass xenon isotopes with $R_{4/2} \approx 2.5$ and low lying 2_2^+ band heads. Using dynamical symmetries to describe the observed collective structures, the X(5) symmetry was proposed for the description of the ^{128,130}Xe isotopes [8–10] while the O(6) symmetry [11] was also invoked for the description of lighter stable Xe isotopes [12]. The O(6) symmetry imposes that the spectroscopic quadrupole moment is null in spite of the large $B(E2)$ and low excitation energy of the 2_1^+state. The low-energy Coulomb excitation experiments performed for the ^{126,128}Xe isotopes suggest, based on the measured $B(E2)$ and spectroscopic quadrupole moments, the deviations from the O(6) symmetry [13]. In [14], the low energy Coulomb excitation of a ^{124}Xe beam on a light target has been performed to investigate the transition probabilities from non yrast states gathered in so-called γ band, three-phonon $K = 0$ band and β band and compared to IBM-1 calculations. As a result it was proposed that the O(6) symmetry in ^{124}Xe is also substantially broken. Safe Coulomb excitation cross sections on a high-Z target is the only method sensitive to the diagonal $E2$ matrix elements of the quadrupole operator of the states with the nonzero spin, i.e., spectroscopic quadrupole moment [15–17]. In this paper, we report the results from the first measurement of spectroscopic quadrupole moments of short-lived excited states in ^{124}Xe obtained by safe Coulomb excitation.

II. EXPERIMENTAL SETUP

The experimental data used in this study was collected in an experiment with a different objective. The main goal of the experiment was the study of the fission yield distribution of the neutron deficient ^{178}Hg isotope populated in the fusion of a ^{124}Xe beam with a ^{54}Fe target deposited on a carbon backing [18,19]. Stable ^{124}Xe beams with energies of 4.03A MeV and 4.11A MeV were accelerated by the GANIL cyclotron complex and delivered to the VAMOS++ AGATA setup in the G1 cave [20–23]. Fission fragments and target-like products were identified in the VAMOS++ magnetic spectrometer and the prompt γ rays were detected in the AGATA tracking array surrounding the target. The Doppler correction was performed on an event-by-event basis using the velocity vector measured by the VAMOS++ instruments and the first interaction points of tracked γ-rays energies deduced from the AGATA OFT tracking algorithm [24].

The analysis of the γ-ray spectrum in AGATA revealed that the Fe target contained an admixture of $^{\text{nat}}$W. The Xe (beam) and W (target) x rays are observed at the energies below 80 keV. The VAMOS++ detection system was optimized for the identification of the fission fragments [18]. Heavy ($A \approx 120$–180) and slow ($\beta \leqslant 10\%$) recoils such as Xe and W were detected at the VAMOS++ focal plane but could not be uniquely identified since they are were stopped within the Bragg peak ionization chambers. Therefore the experiment did not allow to determine the mass for Xe-like or W-like nuclei, however, but provided the mass-over-charge ratio for W-like ions in agreement with masses 182, 184, and 186. The clear and unique identification of the γ ray transitions of ^{182,184,186}W supports the hypothesis of the contamination by $^{\text{nat}}$W of the target.

The VAMOS++ magnetic spectrometer was equipped with a dual position sensitive multi wire proportional chamber (MWPC) detector placed at the entrance of the first quadrupole, providing a precise measurement of the scattering angle with respect to the axis of the incoming beam [22]. Combining this angle with the velocity measurement allowed to obtain an accurate kinematic correlation. Figure 1 shows the corresponding matrix with the experimental kinematic lines for the Xe beam scattered on W ions detected in VAMOS++, the W target ions scattered by the Xe beam detected in VAMOS++ and the Xe beam scattered on the Fe target ions. The corresponding theoretical kinematic lines for Xe+W (red and blue, see later in the text), Xe+Fe (black), and Xe+C (green) are also shown. The combination of the VAMOS++ magnetic rigidity analysis and Doppler correction in AGATA was used to determine the position of the W in the target. First, the charge state measurement of ^{124}Xe scattered into VAMOS++ was optimized from the analysis of the time of flight in the spectrometer. This time of flight was used to determine the velocity between the center of the entrance parallel-plate avalanche counters (PPAC) detector and the stop detector at the focal plane and to deduce the mass over charge ratio. A small correction of this velocity was needed to optimize the Doppler

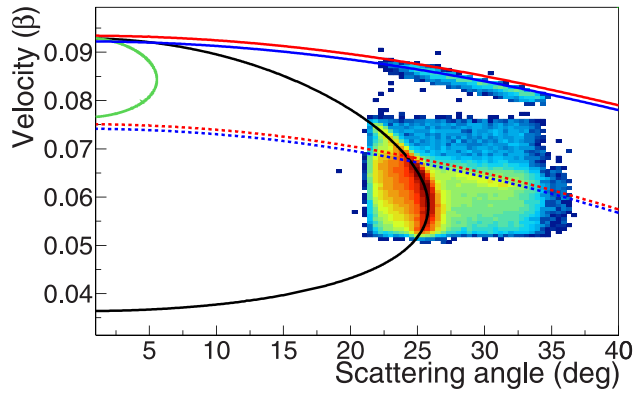

FIG. 1. Kinematic lines (scattering angle as a function of the velocity) measured at the entrance of VAMOS++. Continuous red (blue) shows the Xe beam scattered at maximum (minimum) energy on W detected in VAMOS++; dashed red (blue) shows the W target scattered by the Xe beam at maximum (minimum) energy detected in VAMOS++. Green is the kinematic line for the Xe beam scattered on the carbon backing, excluded by the detection system; black shows Xe beam scattered on the iron target.

correction in AGATA due to the energy loss in the first gas volume of the PPAC. The optimum velocity for Doppler correction was then reported in the two-dimensional (2D) matrix of Fig. 1. The kinematic lines for direct scattering of ^{124}Xe on $^{\text{nat}}$W, at the actual beam energy, are plotted in red. The blue lines show the same calculations assuming that the beam was losing energy in the ^{54}Fe material and ^{12}C backing before scattering on the $^{\text{nat}}$W. The data show a best compatibility with the second hypothesis constraining very well the kinematics of the reactions for the Coulomb excitation analysis.

Figure 2 shows the prompt, Doppler corrected for W, tracked γ-ray spectrum selected on the kinematic lines of the Xe + W reaction confirming the identification of the $^{\text{nat}}$W. The Coulomb excitation of the 2_1^+, 4_1^+, 6_1^+, and 8_1^+ states in ^{182,184,186}W are observed. The reduced intensity of the 2_1^+ decay is due to a shadowing effect of the target chamber arising from the long lifetime of the states. The inelastic scattering on W fulfilled the Cline's criterion of safe Coulomb excitation [25] for the beam energies of 4.03A MeV and 4.11A MeV further slowed down in the Fe target. The inelastic scattering of the Xe beam on the W target is selected from the kinematic lines for two ranges at each energy, between 27.2° and 34.4°

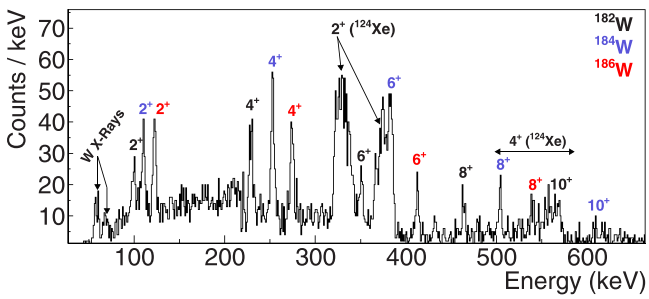

FIG. 2. Prompt γ-ray spectrum following the de-excitation of ^{182,184,186}W after Coulomb excitation measured in AGATA.

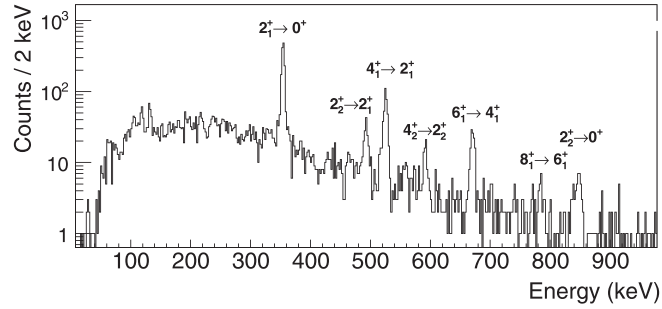

FIG. 3. Prompt γ-ray spectrum following the de-excitation of ^{124}Xe after safe Coulomb excitation at the beam energy of 4.03A MeV.

when ^{124}Xe is measured in VAMOS++ and between 26.9° and 33.4° when $^{\text{nat}}$W is transmitted (see Fig. 1).

III. ANALYSIS AND RESULTS

The prompt Doppler corrected tracked γ-ray spectrum, gated on the ^{124}Xe scattered on $^{\text{nat}}$W events, for the 4.03A MeV beam energy is shown in Fig. 3. The rotational ground-state band was populated up to the 8_1^+ state, the 2_2^+ and 4_2^+ states were also populated. The statistics is further divided

TABLE I. Observed γ-ray transitions in ^{124}Xe with their intensities (without efficiency correction), collected on W target, for ranges of center-of-mass scattering angles used in the Coulomb excitation analysis.

Data set	I_i^π	I_f^π	E_γ (keV)	Counts	Error
4.03A MeV	2_1^+	0_1^+	354	724	30
(45.2°-56.9°)	4_1^+	2_1^+	525	62	10
	6_1^+	4_1^+	670	7	3
	2_2^+	2_1^+	493	16	5
	2_2^+	0_1^+	846	4	2
4.03A MeV	2_1^+	0_1^+	354	559	30
(113.1°-126.1°)	4_1^+	2_1^+	525	253	52
	6_1^+	4_1^+	670	107	12
	8_1^+	6_1^+	783	15	5
	2_2^+	2_1^+	493	84	20
	2_2^+	0_1^+	846	19	5
	4_2^+	2_2^+	591	48	9
4.11A MeV	2_1^+	0_1^+	354	635	30
(45.2°-56.9°)	4_1^+	2_1^+	525	79	12
	2_2^+	2_1^+	493	16	6
4.11A MeV	2_1^+	0_1^+	354	772	35
(113.1°-126.1°)	4_1^+	2_1^+	525	295	20
	6_1^+	4_1^+	670	92	14
	8_1^+	6_1^+	783	17	6
	2_2^+	2_1^+	493	86	13
	2_2^+	0_1^+	846	35	8
	4_2^+	2_2^+	591	53	10

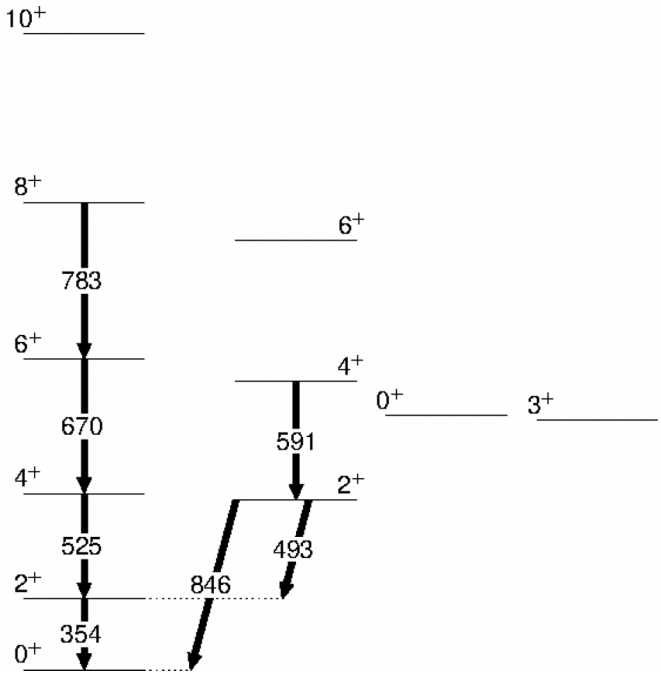

FIG. 4. Partial level scheme of ^{124}Xe with observed transitions. Additional states included in the analysis are also shown.

by ranges in scattering angle to take full advantage of the differential Coulomb excitation sensitivity.

The γ-ray intensities, without efficiency correction, for several bins in scattering angle at different beam energies are reported in Table I. The Coulomb excitation analysis were performed using the least squares fitting code GOSIA [26,27]. The code uses a standard χ^2 function constructed from the measured γ-ray yields and those calculated from a set of electromagnetic matrix elements, both transitional and diagonal, between all states involved in the excitation process. Known spectroscopic data, such as lifetimes of excited states, $\delta(E2/M1)$ mixing and decay branching ratios, were used as additional data points in the minimization procedure. The $2_1^+ \rightarrow 0_1^+$ transition in ^{124}Xe was used for normalization.

The partial level scheme of ^{124}Xe included in the GOSIA minimization is presented in Fig. 4. To enhance the sensitivity, additional inputs such as the 2_1^+, 4_1^+, 6_1^+, 8_1^+, 2_2^+, 4_2^+, and 3_1^+ states lifetimes, the known decay branching ratios of the 2_2^+, 4_2^+, 6_2^+, and 3_1^+ states, the $\delta(E2/M1)$ mixing ratio for the $2_2^+ \rightarrow 2_1^+$, $4_2^+ \rightarrow 4_1^+$, $6_2^+ \rightarrow 6_1^+$, $3_1^+ \rightarrow 2_2^+$, and $3_1^+ \rightarrow 2_1^+$ transitions [28] and the known g factor of the 2_1^+ state [29] were included in the minimization process (see Table II). The kinematic lines in Fig. 1 are selected through the VAMOS++ acceptance. This effect is known for inelastic scattering in VAMOS++ [30] and was taken into account by a proper description of the $(\theta - \phi)$ dependences of the scattering angles in GOSIA as described in [27]. The angular dependence of the setup was validated by the analysis of the differential Coulomb excitation cross section of the 4_1^+, 6_1^+, and 8_1^+ states in ^{182}W. The agreement with the calculated cross sections using the matrix elements published in [31] is excellent demonstrating our control of the angular dependence.

TABLE II. Spectroscopic informations included in the minimization.

I^π	Lifetime τ (ps) [28]
2_1^+	67.51(1.73)
	g factor = 0.23(2) [29]
4_1^+	8.19(23)
6_1^+	1.86(15)
8_1^+	1.13(34)
2_2^+	17.74(3.03)
4_2^+	3.02(1.00)
3_1^+	8.94(1.00)
Transition	Branching ratio [28]
$2_2^+ \rightarrow 2_1^+/2_2^+ \rightarrow 0_1^+$	0.33(8)
$3_1^+ \rightarrow 4_1^+/3_1^+ \rightarrow 2_2^+$	0.13(3)
$3_1^+ \rightarrow 2_2^+/3_1^+ \rightarrow 2_1^+$	0.76(17)
$0_2^+ \rightarrow 2_2^+/0_2^+ \rightarrow 2_1^+$	0.10(5)
$4_2^+ \rightarrow 4_1^+/4_2^+ \rightarrow 2_2^+$	0.44(8)
$4_2^+ \rightarrow 2_2^+/4_2^+ \rightarrow 2_1^+$	0.02(1)
$6_2^+ \rightarrow 6_1^+/6_2^+ \rightarrow 4_2^+$	0.23(3)
$6_2^+ \rightarrow 4_2^+/6_2^+ \rightarrow 4_1^+$	0.10(2)
Transition	$\delta(E2/M1)$ mixing ratio [28]
$2_2^+ \rightarrow 2_1^+$	+8(7)
$3_1^+ \rightarrow 2_2^+$	+0.32(5)
$3_1^+ \rightarrow 2_1^+$	+0.73(6)
$4_2^+ \rightarrow 4_1^+$	+2.3(8)
$6_2^+ \rightarrow 6_1^+$	−0.54(18)

The minimization process was carried out in three steps. First, the 4_2^+, 3_1^+, and 0_2^+ states and their spectroscopic data were excluded from the minimization to obtain a first set of matrix elements reproducing the main transitions. The γ-ray yield of the 4_2^+ state, observed only in two data sets of Table I corresponding to the largest scattering angles, and its additional spectroscopic constrains were added in a second step of the minimization. In Ref. [14], the 0_2^+ and 3_1^+ states were observed and the measured $B(E2)$ were found to be large. Decays from both states were not observed in the present data. Their spectroscopic data were well determined [14,28] and allowed us to investigate the effect of unobserved states in our minimization process. Therefore, in a third step of the minimization, the 0_2^+ and 3_1^+ states with their spectroscopic information were included in the minimization process. As a result, a minimum in χ^2 was obtained for a set of $E2$ and $M1$ matrix elements, including their relative signs, reproducing best the γ-ray intensities for all data sets and known spectroscopic information. Particular care was taken in verifying the uniqueness of the best solution after varying the relative signs of the matrix elements.

The transitional matrix elements allow to calculate the reduced transition probabilities and the spectroscopic quadrupole moments Q_s were deduced from diagonal matrix elements. The results are presented in Tables III and IV. The experimental $B(E2)$ values in Table III labeled with the b symbol are influenced by the 0_2^+ and 3_1^+ states present in the

TABLE III. Reduced transition probabilities in ^{124}Xe obtained in this work and compared to previous data.

I_1^π	I_2^π	$B(E2; I_1 \to I_2)(e^2b^2)$	$B(E2)$ (Wu)	Prev. [14]	IBM-1[14]
2_1^+	0_1^+	$0.212^{+0.006}_{-0.006}$	57.7(16)	57.7(15)[a]	57.7
4_1^+	2_1^+	$0.253^{+0.008}_{-0.008}$	68.8(21)	67.6(19)[a]	85.08
6_1^+	4_1^+	$0.339^{+0.030}_{-0.030}$	92.3(81)	90(18)	96.95
8_1^+	6_1^+	$0.35^{+0.27}_{-0.27}$	95(73)		
2_2^+	0_1^+	$0.0031^{+0.0008}_{-0.0005}$	0.84^{+21}_{-13}	1.45(12)	1.47
2_2^+	2_1^+	$0.135^{+0.020}_{-0.017}$	36.7(54)	64(5)	61.24
4_1^+	2_2^+	$1.0(^{+0.1}_{-1.0}) \times 10^{-3}$	<0.30[b]	92(58)	0.06
4_2^+	2_2^+	$0.244^{+0.055}_{-0.055}$	66(15)[b]	66(12)	48.48
4_2^+	4_1^+	$0.004^{+0.020}_{-0.020}$	<10[b]	35(6)	33.53
4_2^+	2_1^+	$0.0002^{+0.001}_{-0.002}$	<0.5	0.058(11)	0.33
3_1^+	2_1^+	$0.0029^{+0.0006}_{-0.0004}$	0.80(16)	2.33(38)	2.20
3_1^+	2_2^+	$0.033^{+0.011}_{-0.010}$	9(3)	95(19)	65.69
3_1^+	4_1^+	$0.09^{+0.02}_{-0.02}$	24(5)	26(12)	20.71
0_2^+	2_1^+	$0.11^{+0.06}_{-0.06}$	31(17)	13.2(31)	16.12
0_2^+	2_2^+	$0.33^{+0.37}_{-0.21}$	$90(^{+100}_{-57})$	87(21)	76.45

[a]From Ref. [32].
[b]Influenced by the 0_2^+ and 3_1^+ states presence in the GOSIA minimization (see text).

GOSIA minimization. The final error bars include the statistical effects of observed transitions and the systematic effects from the unobserved 0_2^+ and 3^+ states. All the known branching ratio are reproduced within 1σ. The $\delta(E2/M1)$ mixing ratio for the $2_2^+ \to 2_1^+$ and $4_2^+ \to 4_1^+$ transitions are reproduced at 1.5 and 2.6 σ, respectively. All lifetimes are reproduced below 1σ. All γ-ray intensities are reproduced below 2σ except for the $4_1^+ \to 2_1^+$ transition, in the last data set, with a deviation at 3.4 σ.

χ^2 scans were performed for the $E2$ and $M1$ matrix elements connecting the nonyrast states to the ground state band for which no γ transition is observed. The results are presented in Fig. 5. The χ^2 dependence on the $E2$ matrix element between the 4^+ states is weak as revealed by the large error bar. The $M1$ dependence is, however, very strong. Similarly, the χ^2 dependence on the $E2$ matrix element between the 3_1^+ and 2_2^+ states is strong excluding previously measured values. The χ^2 analysis shows that the dependence comes from agreement with the spectroscopic data such as the lifetime and the branching ratio for the 3_1^+ and 2_2^+ states. In the present analysis, the mixing and branching ratio used in the minimization were taken from the evaluated values in [28] as in [14], the experimental values from [12] were used having a significant deviation for the mixing ratio of the $3_1^+ \to 2_2^+$

TABLE IV. Spectroscopic quadrupole moments, Q_s (eb), in ^{124}Xe obtained in this work and compared to ^{126,128,130}Xe.

I^π	^{124}Xe	^{126}Xe [33]	^{128}Xe [33]	^{130}Xe [10]
2_1^+	$-1.60^{+0.22}_{-0.36}$	−0.76(15)	$-0.44^{+0.09}_{-0.12}$	$-0.38^{+0.17}_{-0.14}$
4_1^+	$-1.43^{+0.30}_{-0.20}$	−0.59(12)	−1.04(10)	−0.41(12)
6_1^+	$-0.67^{+0.60}_{-0.20}$			

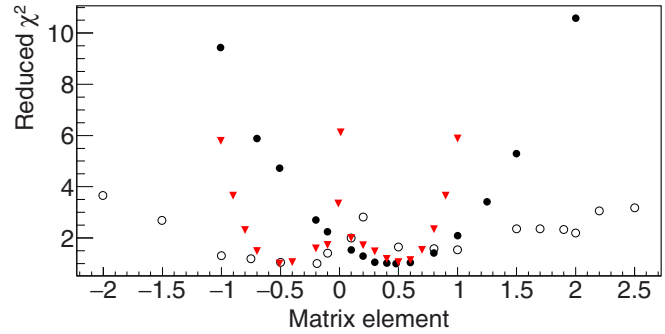

FIG. 5. χ^2 scans for the $E2$ the $3^+ \to 2_2^+$ (full circles) and $4_2^+ \to 4_1^+$ (open circles) (eb) and $M1$ $4_2^+ \to 4_1^+$ (red triangle) (μ_N) matrix elements.

transition. A χ^2 scan for the 2_1^+ state diagonal matrix element is shown in Fig. 6. In the figure, only this matrix element was permitted to vary, keeping the others at their nominal values. This χ^2 scan is shown for illustration and cannot be used for the final error evaluation. The later shown in Tables III and IV is obtained using the full GOSIA procedure [27].

The stability of the solution was investigated under different assumptions as shown in Fig. 7. The diagonal matrix element of the first 2^+ state was found very stable under these different constraints. In Table III, three reduced transition probabilities are significantly different from the previous measurement. The $B(E2, 4_1^+ \to 2_2^+)$ was found much smaller than the previous experimental value but becomes compatible with the IBM-1 calculations having a remarkable agreement with the experimental data. The $B(E2, 3_1^+ \to 2_2^+)$ and $B(E2, 4_2^+ \to 4_1^+)$ were also found much smaller with large error bars and deviate from the IBM-1 calculations.

The deduced spectroscopic quadrupole moments for the 2_1^+, 4_1^+, and 6_1^+ states are shown in Table III. They are large and negative underlining the prolate axial deformation of the ground state band with an axial deformation parameter $\langle\beta_2\rangle \approx 0.3$. The matrix elements were further analyzed using the quadrupole sum rules approach [25]. This method relates experimentally determined $E2$ matrix elements to

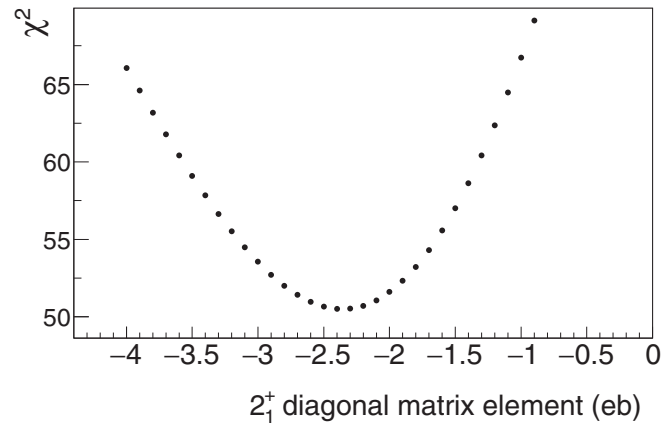

FIG. 6. χ^2 scan on the 2_1^+ diagonal matrix element. Only this matrix element was permitted to vary, others remain fixed.

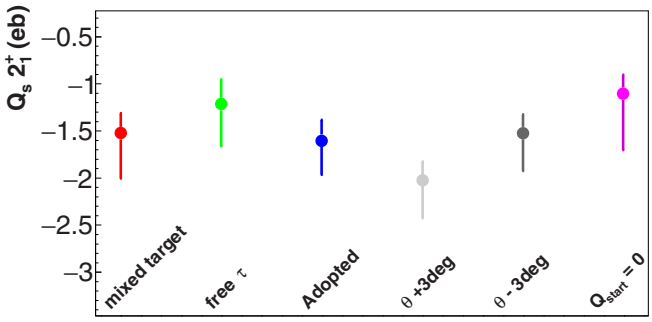

FIG. 7. Stability of the solution under different assumptions. In red, ^{nat}W is considered as mixed in Fe, i.e., cross sections are integrated over the full Fe thickness. In blue, the W is facing VAMOS, i.e., cross sections are calculated at the lowest beam energy (Table III). The light (dark) gray assumes a misalignment in scattering angle of ±3 degrees in the laboratory frame, respectively. In violet, the minimization is forced to low Q_s and constrained released for final solution. In green, all lifetimes are a free parameter of the minimization.

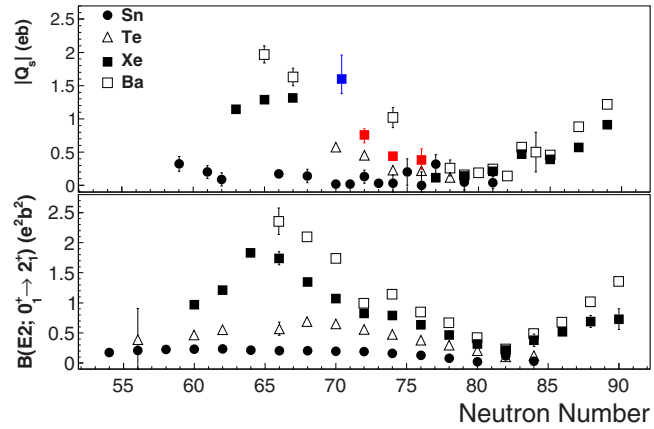

FIG. 8. Top: Spectroscopic quadrupole moment systematics as a function of the neutron number for Sn, Te, Xe, and Ba elements. The present work is highlighted in blue for ^{124}Xe. The recent measurements in $^{126-130}$Xe [10,33] are shown in red. Bottom: Reduced transition probability systematics as a function of the neutron number for Sn, Te, Xe, and Ba elements.

deformation parameters, defined in the intrinsic frame of the nucleus, by constructing quadrupole invariants $\langle \mathcal{Q}^2 \rangle$ and $\langle \mathcal{Q}^3 \cos(3\delta) \rangle$. The $\mathcal{Q}$ parameter describes the magnitude of the deformation, while the δ parameter measures triaxiality. To determine the $\langle \mathcal{Q}^2 \rangle$ invariant for a 0^+ state, it is necessary to measure absolute values of all $E2$ matrix elements that couple the state in question with low-lying 2^+ states. To obtain the triaxiality parameter, $\langle \cos(3\delta) \rangle$, more experimental information is needed, namely transitional matrix elements, along with their relative signs, between the state in question and 2^+ states, those coupling the 2^+ states one to another, as well as diagonal $E2$ matrix elements of the 2^+ states. As shown in [34], the $\langle \mathcal{Q}^2 \rangle$ invariant for the ground state in even-even nuclei is dominated by the contribution of the $\langle 0_1^+ \| E2 \| 2_1^+ \rangle$ matrix element. The $\langle 0_1^+ \| E2 \| 2_2^+ \rangle$ and $\langle 0_1^+ \| E2 \| 2_3^+ \rangle$ matrix elements contributed less to the final $\mathcal{Q}^2$ value for the ground state. The situation is more complex for the higher-order quadrupole invariant $\langle \mathcal{Q}^3 \cos(3\delta) \rangle$. Reference [35] demonstrates that this invariant can be derived with a good accuracy using only four matrix elements: $\langle 0_1^+ \| E2 \| 2_1^+ \rangle$, $\langle 2_1^+ \| E2 \| 2_1^+ \rangle$, $\langle 2_1^+ \| E2 \| 2_2^+ \rangle$, and $\langle 2_2^+ \| E2 \| 0_1^+ \rangle$. In the particular case of γ unstable deformed nuclei, the contribution of both 2_2^+ and 2_3^+ must be included. For ^{124}Xe, matrix elements between the 2_1^+ and 2_2^+ states and the ground state were determined. All reduced transition probabilities between the 2_3^+ and 0_2^+ states and the observed states are known from Ref. [14] and can be translated in $E2$ matrix elements with unknown sign. All combinations of signs were tested giving rise to systematic errors in our calculations. The sum rules yield for the 0_1^+ state $\langle \mathcal{Q}^2 \rangle = 1.07(\pm 2\,\text{stat})(\pm 1\,\text{syst})e^2b^2$ and $\langle \cos(3\delta) \rangle = 1.7(\pm 5\,\text{stat})(\pm 3\ \text{syst})$.The $\langle \mathcal{Q}^2 \rangle$ was found large as expected for a rotational ground state band. Its value is similar to the one measured for the 0_1^+ state in ^{126}Xe and ^{128}Xe [33]. However, the $\langle \cos(3\delta) \rangle$ parameter is found two times larger than the corresponding value in ^{126}Xe and ^{128}Xe [33] supporting the fast increase of axiallity toward midshell. The second invariant can also be translated in the deformation parameter $\gamma \approx 1/3 \arccos\langle \cos(3\delta) \rangle$. With $\langle \cos(3\delta) \rangle = 1.7(5)(3)$, the deformation parameter γ is null underlining the pure axial symmetry of the 0_1^+ state and thus supporting a significant breaking of the O(6) symmetry.

IV. DISCUSSION

The presented result can be placed within a wider systematics. In Fig. 8, the systematic of the reduced transition probabilities for the first 2^+, $B(E2, 2_1^+ \rightarrow 0_1^+)$, is shown as a function of the neutron number for the even-mass isotopes of Sn, Te, Xe, and Ba. The $N = 82$ shell closure is well marked with a minimum of $B(E2)$. When removing neutrons, the collectivity follow a smooth increase toward midshell having a maximum at $N = 66$–68 and an amplitude proportional to the number of proton pairs outside of the $Z = 50$ shell closure. The spectroscopic quadrupole moment obtained for ^{124}Xe (blue square) is compared to the spectroscopic quadrupole moments of odd-mass Xe (full squares), Ba, Te, and Sn ground states and 2_1^+ states for the even-mass isotopes, where known. The recent measurement in $^{126-130}$Xe [10,33] are shown in red squares. The newly presented data points fit both the systematics of the $^{117-121}$Xe isotopes with large values reaching a maximum at $N = 70$, indicating large deformation, followed by the decrease as function of the neutron number, in line with the systematic of $^{126-130}$Xe. From ^{131}Xe, approaching the $N = 82$ neutron shell closure, the spectroscopic quadrupole moments are reduced. The systematics suggests a fast decrease of the β deformation in the Xe chain, probably associated to an increase of triaxiality as suggested in [10]. The spectroscopic quadrupole moment for the 2_1^+ and 4_1^+ states are compared for $^{124-130}$Xe in Table III; The continuous increase of the Q_s of the 2_1^+ state from ^{130}Xe to ^{124}Xe is clearly visible. The analysis for the 4_1^+ is less evident. The value for ^{124}Xe is significantly larger than the one reported for the heavier isotopes suggesting an axially deformed state.

The large values of the spectroscopic quadrupole moments support the breaking of the O(6) symmetry in ^{124}Xe as suggested by [14] and favor the SU(3) symmetry for the ground state band. The exact O(6) symmetry is an ideal case of γ-unstable rotor for which $\langle\cos(3\delta)\rangle$ equals zero. Any small admixture of other symmetries will lead to $\langle\cos(3\delta)\rangle \neq 0$. ^{124}Xe has drawn some attention since its level scheme is in remarkable agreement with the IBM-1 model calculations having a large triaxial degree of freedom and with the typical spectrum for a nucleus exhibiting the O(6) symmetry [12,36]. Even if the agreement with the level scheme is very good, the comparison with the transition probabilities has shown that the O(6) symmetry is substantially broken [14] and it is confirmed by the present spectroscopic quadrupole moments.

^{124}Xe is collective but with a $R_{42} = E(4_1^+)/E(2_1^+)$ ratio equal to 2.48, it cannot be considered as a rotational nucleus at the limit of SU(3). In [37], a large survey of the correlation between experimental spectroscopic quadrupole moments Q_s, $B(E2)$ and R_{42} ratio is presented. X(5) symmetry like nuclei such as $^{148-150}$Nd, ^{152}Sm and ^{154}Gd present large spectroscopic quadrupole moments with respect to their respective R_{42} and $B(E2, 2_1^+ \rightarrow 0_1^+)$ values. In this survey a R_{QB} parameter was defined from the 2_1^+ spectroscopic quadrupole moments and $B(E2)$ to the ground state. The ^{124}Xe value is $R_{QB} = 1.46(^{+21}_{-46})$. It lies at the extreme of the R_{QB} systematics along the nuclear chart with the $^{148-150}$Nd or $^{200-202}$Hg which are just below and above the rotational region where $R_{QB} \approx 1$. The systematic in [37] shows that these large R_{QB} are between Nd and Os elements. The present results suggest that it could be extended up to Xe and such cases remain to be understood. ^{124}Xe has extraordinary similarities with the X(5)-like nucleus ^{148}Nd. The ^{124}Xe (^{148}Nd) Q_s equals -1.51^{+21}_{-48} [$-1.46(13)$] (eb), $B(E2, 2_1^+ \rightarrow 0_1^+)$ equals 57.7(16) [57.5(13)] (Wu), and R_{42} equals 2.48 (2.49), respectively. ^{148}Nd was investigated in detail by safe Coulomb excitation [38]. Similarly to ^{124}Xe, ^{148}Nd presents a coexistence below 1.5 MeV excitation energy of a rotational ground state band, an octupole collective band, a β band and a γ band. The fair similarities between the in-band $E2$ matrix elements for the ground state bands and for γ bands and interband $E2$ matrix elements between the two collective bands suggest that both nuclei can be described as deformed axial nuclei and deviation from the rotational behavior can be accounted for by including the coupling between rotational and vibrational modes [38]. The detailed coupling between the quadrupole rotation and the octupole vibration requires further experimental verification in ^{124}Xe.

V. CONCLUSION

The spectroscopic quadrupole moments for the 2_1^+, 4_1^+, and 6_1^+ states have been determined in ^{124}Xe using the safe Coulomb excitation technique using a target with high Z. The values found are large and negative underlining a large prolate axial deformation. These large spectroscopic quadrupole moments support that the O(6) symmetry is substantially broken. A more microscopical approach would be necessary to fully understand the collective behavior at low angular momentum in the midshell Xe isotopes. The large measured spectroscopic quadrupole moments lie at the limits of the nuclear collective models.

ACKNOWLEDGMENTS

We acknowledge the GANIL facility for provision of heavy-ion beams and we would like to thank J. Goupil, G. Fremont, L. Ménager, J. Ropert, C. Spitaels for assistance in using the G1 beam line and its instrumentation. This work was supported by STFC(UK). This research was also supported by the OASIS Project No. ANR-17-CE31-0026, by the U.S. Department of Energy, Office of Science, Office of Nuclear Physics, under Contract No. DE-AC02-06CH11357, by the European Regional Development Fund with Contract No. GINOP-2.3.3-15-2016-00034, and by the Spanish Ministerio de Ciencia e Innovación under Contract No. PID2020-118265GB-C41. Work partially supported by Grants No. FPA2017-84756-C4, PID2020-118265GB-C4 by MCIN/AEI/10.13039/501100011033, PROMETEO/2019/005 by Generalitat Valenciana and by the FEDER EU funds.

[1] G. Jakob, N. Benczer-Koller, G. Kumbartzki, J. Holden, T. J. Mertzimekis, K.-H. Speidel, R. Ernst, A. E. Stuchbery, A. Pakou, P. Maier-Komor, A. Macchiavelli, M. McMahan, L. Phair, and I. Y. Lee, Phys. Rev. C **65**, 024316 (2002).

[2] B. Pritychenko, J. Choquette, M. Horoi, B. Karamy, and B. Singh, At. Data Nucl. Data Tables **98**, 798 (2012).

[3] M. Sandzelius, B. Hadinia, B. Cederwall, K. Andgren, E. Ganioğlu, I. G. Darby, M. R. Dimmock, S. Eeckhaudt, T. Grahn, P. T. Greenlees, E. Ideguchi, P. M. Jones, D. T. Joss, R. Julin, S. Juutinen, A. Khaplanov, M. Leino, L. Nelson, M. Niikura, M. Nyman *et al.*, Phys. Rev. Lett. **99**, 022501 (2007).

[4] W. F. Mueller, M. P. Carpenter, J. A. Church, D. C. Dinca, A. Gade, T. Glasmacher, D. T. Henderson, Z. Hu, R. V. F. Janssens, A. F. Lisetskiy, C. J. Lister, E. F. Moore, T. O. Pennington, B. C. Perry, I. Wiedenhöver, K. L. Yurkewicz, V. G. Zelevinsky, and H. Zwahlen, Phys. Rev. C **73**, 014316 (2006).

[5] G. de Angelis, A. Gadea, E. Farnea, R. Isocrate, P. Petkov, N. Marginean, D. Napoli, A. Dewald, M. Bellato, A. Bracco, F. Camera, D. Curien, M. D. Poli, E. Fioretto, A. Fitzler, S. Kasemann, N. Kintz, T. Klug, S. Lenzi, S. Lunardi *et al.*, Phys. Lett. B **535**, 93 (2002).

[6] A. Davydov and G. Filippov, Nucl. Phys. **8**, 237 (1958) .

[7] L. Wilets and M. Jean, Phys. Rev. **102**, 788 (1956).

[8] L. Coquard, N. Pietralla, T. Ahn, G. Rainovski, L. Bettermann, M. P. Carpenter, R. V. F. Janssens, J. Leske, C. J. Lister, O. Möller, W. Rother, V. Werner, and S. Zhu, Phys. Rev. C **80**, 061304(R) (2009).

[9] R. M. Clark, M. Cromaz, M. A. Deleplanque, M. Descovich, R. M. Diamond, P. Fallon, I. Y. Lee, A. O. Macchiavelli, H. Mahmud, E. Rodriguez-Vieitez, F. S. Stephens, and D. Ward, Phys. Rev. C **69**, 064322 (2004).

[10] L. Morrison, K. Hadyńska-Klęk, Z. Podolyák, D. T. Doherty, L. P. Gaffney, L. Kaya, L. Próchniak, J. Samorajczyk-Pyśk, J. Srebrny, T. Berry, A. Boukhari, M. Brunet, R. Canavan, R. Catherall, S. J. Colosimo, J. G. Cubiss, H. De Witte, C. Fransen,

E. Giannopoulos, H. Hess *et al.*, Phys. Rev. C **102**, 054304 (2020).
[11] A. Arima and F. Iachello, Phys. Rev. Lett. **40**, 385 (1978).
[12] V. Werner, H. Meise, I. Wiedenhöver, A. Gade, and P. von Brentano, Nucl. Phys. A **692**, 451 (2001).
[13] S. Kisyov, C. Y. Wu, J. Henderson, A. Gade, K. Kaneko, Y. Sun, N. Shimizu, T. Mizusaki, D. Rhodes, S. Biswas, A. Chester, M. Delvin, P. Farris, A. Hill, J. Li, E. Rubino, and D. Weisshaar, Evolution of collectivity in ^{126,128}Xe studied in Coulomb excitation measurements, *15th International Conference on Nuclear Data for Science and Technology (ND2022)* (U. S. Department of Energy, 2022).
[14] G. Rainovski, N. Pietralla, T. Ahn, L. Coquard, C. Lister, R. Janssens, M. Carpenter, S. Zhu, L. Bettermann, J. Jolie, W. Rother, R. Jolos, and V. Werner, Phys. Lett. B **683**, 11 (2010).
[15] K. Alder and A. Winther, Phys. Rev. **91**, 1578 (1953).
[16] K. Alder and A. Winther, Phys. Rev. **96**, 237 (1954).
[17] K. Alder and A. Winter, *Theory of Coulomb Excitation with Heavy Ions* (North Holland, Amsterdam, 1974).
[18] C. Schmitt, A. Lemasson, K.-H. Schmidt, A. Jhingan, S. Biswas, Y. H. Kim, D. Ramos, A. N. Andreyev, D. Curien, M. Ciemala, E. Clément, O. Dorvaux, B. De Canditiis, F. Didierjean, G. Duchêne, J. Dudouet, J. Frankland, B. Jacquot, C. Raison, D. Ralet *et al.*, Phys. Rev. Lett. **126**, 132502 (2021).
[19] A. Jhingan, C. Schmitt, A. Lemasson, S. Biswas, Y. H. Kim, D. Ramos, A. N. Andreyev, D. Curien, M. Ciemała, E. Clément, O. Dorvaux, B. De Canditiis, F. Didierjean, G. Duchêne, J. Dudouet, J. Frankland, G. Frémont, J. Goupil, B. Jacquot, C. Raison *et al.*, Phys. Rev. C **106**, 044607 (2022).
[20] E. Clément *et al.*, Nucl. Instrum. Methods Phys. Res. A **855**, 1 (2017).
[21] S. Akkoyun *et al.*, Nucl. Instrum. Methods Phys. Res. A **668**, 26 (2012).
[22] M. Vandebrouck, A. Lemasson, M. Rejmund, G. Fremont, J. Pancin, A. Navin, C. Michelagnoli, J. Goupil, C. Spitaels, and B. Jacquot, Nucl. Instrum. Methods Phys. Res. A **812**, 112 (2016).
[23] M. Rejmund, B. Lecornu, A. Navin, C. Schmitt, S. Damoy, O. Delaune, J. Enguerrand, G. Fremont, P. Gangnant, L. Gaudefroy, B. Jacquot, J. Pancin, S. Pullanhiotan, and C. Spitaels, Nucl. Instrum. Methods Phys. Res. A **646**, 184 (2011).
[24] A. Lopez-Martens, K. Hauschild, A. Korichi, J. Roccaz, and J.-P. Thibaud, Nucl. Instrum. Methods Phys. Res. A **533**, 454 (2004).
[25] D. Cline, Annu. Rev. Nucl. Part. Sci. **36**, 683 (1986).
[26] T. Czosnyka, D. Cline, and C. Y. Wu, Bull. Am. Phys. Soc. **28**, 745 (1983).
[27] M. Zielińska, L. P. Gaffney, K. Wrzosek-Lipska, E. Clément, T. Grahn, N. Kesteloot, P. Napiorkowski, J. Pakarinen, P. Van Duppen, and N. Warr, Euro. Phys. J. A **52**, 99 (2016).
[28] J. Katakura and Z. Wu, Nucl. Data Sheets **109**, 1655 (2008).
[29] D. M. Gordon, L. S. Eytel, H. de Waard, and D. E. Murnick, Phys. Rev. C **12**, 628 (1975).
[30] C. Plaisir, L. Gaudefroy, V. Méot, A. Blanc, J. M. Daugas, O. Roig, N. Arnal, T. Bonnet, F. Gobet, F. Hannachi, M. Tarisien, M. Versteegen, T. Roger, M. Rejmund, A. Navin, C. Schmitt, G. Fremont, J. Goupil, J. Pancin, C. Spitaels *et al.*, Phys. Rev. C **89**, 021302(R) (2014).
[31] C. Wu, D. Cline, E. Vogt, W. Kernan, T. Czosnyka, K. Helmer, R. Ibbotson, A. Kavka, B. Kotlinski, and R. Diamond, Nucl. Phys. A **533**, 359 (1991).
[32] B. Saha, A. Dewald, O. Möller, R. Peusquens, K. Jessen, A. Fitzler, T. Klug, D. Tonev, P. von Brentano, J. Jolie, B. J. P. Gall, and P. Petkov, Phys. Rev. C **70**, 034313 (2004).
[33] S. Kisyov, C. Y. Wu, J. Henderson, A. Gade, K. Kaneko, Y. Sun, N. Shimizu, T. Mizusaki, D. Rhodes, S. Biswas, A. Chester, M. Devlin, P. Farris, A. M. Hill, J. Li, E. Rubino, and D. Weisshaar, Phys. Rev. C **106**, 034311 (2022).
[34] J. Srebrny *et al.*, Int. J. Mod. Phys. E **20**, 422 (2011).
[35] W. Andrejtscheff and P. Petkov, Phys. Lett. B **329**, 1 (1994).
[36] J. A. Cizewski, R. F. Casten, G. J. Smith, M. L. Stelts, W. R. Kane, H. G. Börner, and W. F. Davidson, Phys. Rev. Lett. **40**, 167 (1978).
[37] Y. Sharon, N. Benczer-Koller, G. Kumbartzki, L. Zamick, and R. Casten, Nucl. Phys. A **980**, 131 (2018).
[38] R. Ibbotson, C. White, T. Czosnyka, P. Butler, N. Clarkson, D. Cline, R. Cunningham, M. Devlin, K. Helmer, T. Hoare, J. Hughes, G. Jones, A. Kavka, B. Kotlinski, R. Poynter, P. Regan, E. Vogt, R. Wadsworth, D. Watson, and C. Wu, Nucl. Phys. A **619**, 213 (1997).